J|A|C|S ARTICLES

Published on Web 09/22/2010

The Thermosalient Phenomenon. "Jumping Crystals" and Crystal Chemistry of the Anticholinergic Agent Oxitropium Bromide

Željko Skoko,[†,#] Sharona Zamir,[‡,¶] Panče Naumov,*[,†] and Joel Bernstein*[,‡]

Department of Material and Life Science, Graduate School of Engineering, Osaka University, 2-1 Yamada-oka, Suita 565-0871, Osaka, Japan, and Department of Chemistry, Ben-Gurion University of the Negev, Beer Sheva 84105, Israel

Received June 23, 2010; E-mail: npance@wakate.frc.eng.osaka-u.ac.jp; yoel@bgu.ac.il

Abstract: The anticholinergic agent oxitropium bromide possesses rich crystal chemistry, most remarkably exhibiting a strong *thermosalient effect* ("jumping crystal" effect), a mechanical property with potential applications in organic-based actuators. The thermosalient effect, manifested in forceful jumps of up to several centimeters, was investigated by a combination of structural, microscopic, spectroscopic, and thermoanalytical techniques, providing data on which to base a proposed mechanism for the phenomenon. Direct observation of the effect in a single crystal and structure determination of both phases revealed that the jumping of the crystals is a macroscopic manifestation of a highly anisotropic change in the cell volume. The cell distortion is accompanied by a conformational change of the oxitropium cation, which triggers increased separation between the ion pairs in the lattice at nearly identical separation between the cation and the anion within each ion pair. At the molecular level, the cation acts as a molecular shuttle composed of two rigid parts (epoxy-aza-tricyclic-nonyl portion and phenyl ring) that are bridged by a flexible ester linkage. The structure of the rigid, inert aza-tricyclic portion remains practically unaffected by the temperature, suggesting a mechanism in which the large, thermally accumulated strain is transferred over the ester bridge to the phenyl ring, which rotates to trigger the phase transition. Mechanistic details of the higher temperature solid-state phenomena are also presented. The high-temperature phase can also be obtained by grinding or UV irradiation of the room-temperature phase. In addition, if it is irradiated with UV light in the presence of KBr, the high-temperature phase undergoes intramolecular photochemical rearrangement. Heating the high-temperature phase to slightly below the melting temperature results in an additional solid-state reaction that results in the conversion of the salt to a mixture of neutral compounds.

1. Introduction

In the course of developing it for utilization as a pharmaceutically active ingredient in the treatment of asthma and other bronchial disorders,[1−4] oxitropium bromide, first synthesized in the 1950s,[5] was found to undergo a dimorphic single-crystal-to-single-crystal phase transition.[6] Initial hot-stage microscopic experiments to investigate the nature of this phase transition[7] immediately indicated that the transition is an example of the *thermosalient phenomenon*, occasionally colloquially referred to as "jumping crystals".[8−17]

† Osaka University.
‡ Ben-Gurion University of the Negev.
# On leave from Physics Department, Faculty of Science, University of Zagreb, Croatia.
¶ Presently at Chemagis Ltd., Israel.

(1) Flohr, E.; Bischoff, K. O. *Respiration* **1979**, *38*, 98–104.
(2) Kneubuhler, H. R.; Kyd, K.; Benoit, R. C.; Scherrer, M. *Schweiz. Med. Wochenschr.* **1980**, *110*, 812–816.
(3) (a) Peel, E. T.; Anderson, G. *Thorax* **1984**, *39*, 453–456. (b) Peel, E. T.; Anderson, G.; Cheong, B.; Broderick, N. *Eur. J. Respir. Dis.* **1984**, *65*, 106–108.
(4) (a) Bozung, K.-H.; Pairet, M.; Reichl, R.; Walland, A. U.S. Patent Appl. 20020179087. (b) Bundschuh, D.; Wollin, S.-L.; Weimar, C. U.S. Patent Appl. 20060147382. (c) Weil, H.-H.; Daab, O. U.S. Patent 6,413,497. (d) Bundschuh, D.; Wollin, S.-L.; Weimar, C. Canadian Patent Appl. 2519682.
(5) Moffat, R. B.; Aspergren, B. D. *J. Am. Chem. Soc.* **1956**, *78*, 3448–3453.
(6) Greenwod, D. J., private communication, 1987.
(7) Zamir, S.; Bernstein, J.; Greenwood, D. J. *Mol. Cryst. Liq. Cryst.* **1994**, *242*, 193–200. Many additional details, some of which are reported here, may also be found in the Ph.D. thesis (in Hebrew): Zamir, S. Ph.D. thesis, Ben-Gurion University of the Negev, 1995.
(8) Etter, M. C.; Siedle, A. R. *J. Am. Chem. Soc.* **1983**, *105*, 641−643.
(9) Gigg, J.; Gigg, R.; Payne, S.; Conant, R. *J. Chem. Soc., Perkin Trans. 1* **1987**, 2411–2414.
(10) Ding, J.; Herbst, R.; Praefcke, K.; Kohne, B.; Saenger, W. *Acta Crystallogr.* **1991**, *B47*, 739–742.
(11) Steiner, T.; Hinrichs, W.; Saenger, W. *Acta Crystallogr.* **1993**, *B49*, 708–718.
(12) Fernandes, M. A.; Levendis, D. C.; Schoening, F. R. L. *Acta Crystallogr.* **2004**, *B60*, 300–314.
(13) Corbett, J. M.; Dickman, M. H. *Acta Crystallogr.* **1996**, *C52*, 1851–1853.
(14) Crottaz, O.; Kubel, F.; Schmid, H. *J. Mater. Chem.* **1997**, *7*, 143–146.
(15) Lieberman, H. F.; Davey, R. J.; Newsham, D. M. T. *Chem. Mater.* **2000**, *12*, 490–494.
(16) Kaftory, M.; Botoshansky, M.; Kapon, M.; Shteiman, V. *Acta Crystallogr.* **2001**, *B57*, 791–799.

The recent revival of the interest in thermally induced[7−22] and photoinduced[18,23−46] mechanical effects in solids was triggered by their potential as a prospective material basis for fabrication of efficient actuators—mechanical devices which are capable of converting thermal (kinetic) or light energy into motion or mechanical work at a macroscopic level.[47−49] While such effects have been known for a number of azobenzene-containing polymers[24−28] and liquid-crystal-like materials,[29−33] only a few examples of photomechanical and thermomechanical effects which retain the integrity of single crystals have been reported. Besides solid-to-solid phase transitions,[7−15,17,50] at the molecular level these examples include electrocyclization and ring-opening of diarylethenes,[34−38] [4+4] photoinduced cycloadditions of anthracenes,[39−43] and [2+2] photodimerizations of proximate, parallel double bonds.[44−46] Contrary to amorphous or liquid crystalline materials, which can readily absorb the macroscopic mechanical stress that builds up during the microscopic deformations, similar processes are usually destructive to single crystals. The critical requirement for preservation of the integrity of a single crystalline phase during phase transitions or (photo)chemical reactions that are manifested by macroscopic mechanical effects is that the stress exerted on the lattice by such processes is highly reconstructive.[51,52] In fact, any substantial differences between the molecular packing of the two phases would result in an irreversible change of the original crystal lattice, occasionally followed by nucleation and growth of macroscopic domains of the product lattice.[53−56]

Specifically, when heated or cooled, the thermosalient solids undergo sharp phase transitions accompanied by a sudden, markedly large and anisotropic change in their cell volume, causing the crystals to jump to heights of several times their size. The potential for practical applications of the thermosalient effect for thermal-to-mechanical energy conversion (*vide infra*) requires elucidation of the mechanism and detailed understanding of the relationship between structural changes at a molecular level and their expression at the macrostructural level. In most cases, however, practical reasons—such as decreased crystal quality, latent/permanent crystal deformation, or sublimation—have rendered the structural analysis of the product (usually, the high-temperature phase) fraught with substantial difficulties. As a consequence, virtually no experimental evidence exists on the atomic-scale mechanisms driving these transitions. By employing a variety of analytical techniques, we provide herein a detailed experimental study of the thermosalient effect of oxitropium bromide and a proposed mechanism for the phenomenon based on those data. Moreover, the analytical procedures revealed two other solid-state reactions, which are also described here.

One of the first reported examples of the thermosalient effect was (phenylazophenyl)palladium hexaflouroacetylacetonate.[8] When heated to 363.2(1) K, the needle-like crystals of this material undergo a sudden, discontinuous expansion of about 10% along the needle axis without any apparent change in their width. If heated on only one face, the crystals literally fly off their basis as a result of the colossal mechanical strain that develops. The subsequent gradual but permanent color change from yellow to red is accompanied by increased disorder of the lattice, as revealed by Weissenberg X-ray photographs. This phase transition is irreversible, and the two phases exhibit different X-ray powder patterns and optical properties. The proposed mechanism for this transformation is that the alternating molecular stacks of the low-temperature phase slip together by moving along the [011] direction, which closely corresponds to the long axis of the molecules, as in a martensitic transformation.[57]

(17) Boese, R.; Cammack, J. K.; Matzger, A. J.; Pflug, K.; Tolman, W. B.; Vollhardt, K. P. C.; Weidman, T. W. *J. Am. Chem. Soc.* **1997**, *119*, 6757–6773.
(18) *Reactivity of Solids: Past, Present and Future*; Boldyrev, V. V., Ed.; Blackwell: Oxford, 1996.
(19) Boldyrev, V. V. *Annu. Rev. Mater. Sci.* **1979**, *9*, 455–469.
(20) Brown, M. E.; Dollimore, D.; Galwey, A. K. *Comprehensive Chemical Kinetics*, Vol. 22; Elsevier: Amsterdam, 1980.
(21) Sestak, J. *Thermophysical Properties of Solids*; Elsevier: Amsterdam, 1984.
(22) Bernstein, J. *Polymorphism in Molecular Crystals*; Oxford University Press: Oxford, 2002; p 223.
(23) *Photoinduced Phase Transitions*; Nasu, K., Ed.; World Scientific: Singapore, 2004.
(24) Barrett, C. J.; Mamiya, J.; Yager, K. G.; Ikeda, T. *Soft Matter* **2007**, *3*, 1249–1261.
(25) Koshima, H.; Ojima, N.; Uchimoto, H. *J. Am. Chem. Soc.* **2009**, *131*, 6890–6891.
(26) Finkelmann, H.; Nishikawa, E.; Pereira, G. G.; Warner, M. *Phys. Rev. Lett.* **2001**, *87*, 015501.
(27) Yu, Y.; Nakano, M.; Shishido, A.; Shiono, T.; Ikeda, T. *Chem. Mater.* **2004**, *16*, 1637–1643.
(28) Ikeda, T.; Nakano, M.; Yu, Y.; Tsutsumi, O.; Kanazawa, A. *Adv. Mater.* **2003**, *15*, 201–205.
(29) Yamada, M.; Kondo, M.; Mamiya, J.; Yu, Y.; Kinoshita, M.; Barrett, C. J.; Ikeda, T. *Angew. Chem., Int. Ed.* **2008**, *47*, 4986–4988.
(30) Uchino, K.; Aizawa, M. *Jpn. J. Appl. Phys.* **1985**, *24*, 139–141.
(31) Welker, D. J.; Kuzyk, M. G. *Appl. Phys. Lett.* **1995**, *66*, 2792–2794.
(32) Rochon, P.; Batalla, E.; Natansohn, A. *Appl. Phys. Lett.* **1995**, *66*, 136–138.
(33) Kim, D. Y.; Tripathy, S. K.; Li, L.; Kumar, J. *Appl. Phys. Lett.* **1995**, *66*, 1166–1168.
(34) Kobatake, S.; Takami, S.; Muto, H.; Ishikawa, T.; Irie, M. *Nature* **2007**, *446*, 778–781.
(35) Colombier, I.; Spagnoli, S.; Corval, A.; Baldeck, P. L.; Giraud, M.; Léaustic, A.; Yu, P. *Mol. Cryst. Liq. Cryst.* **2005**, *431*, 495–499.
(36) Irie, M. *Chem. Rev.* **2000**, *100*, 1685–1716.
(37) Irie, M.; Kobatake, S.; Horichi, M. *Science* **2001**, *291*, 1769–1772.
(38) Morimoto, M.; Irie, M. *Chem. Commun.* **2005**, *31*, 3895–3905.
(39) Al-Kaysi, R. O.; Müller, A. M.; Bardeen, C. J. *J. Am. Chem. Soc.* **2006**, *128*, 15938–15939.
(40) Al-Kaysi, R. O.; Bardeen, C. J. *Adv. Mater.* **2007**, *19*, 1276–1280.
(41) Kaupp, G. *Angew. Chem., Int. Ed. Engl.* **1992**, *31*, 595–598.
(42) Keating, A. E.; Garcia-Garibay, M. A. In *Organic and Inorganic Photochemistry, II*; Ramamurthy, V., Schanze, K. S., Eds.; Marcel Dekker: New York, 1998; p 195.
(43) Turowska-Tyrk, I. *J. Phys. Org. Chem.* **2004**, *17*, 837–847.
(44) Naumov, P.; Kowalik, J.; Solntsev, K. M.; Baldridge, A.; Moon, J.-S.; Kranz, C.; Tolbert, L. M. *J. Am. Chem. Soc.* **2010**, *132*, 5845–5857.
(45) Tanaka, K.; Mochizuki, E.; Yasui, N.; Kai, Y.; Miyahara, I.; Hirotsu, K.; Toda, F. *Tetrahedron* **2000**, *56*, 6853–6865.
(46) Friščić, T.; MacGillivray, L. R. *Z. Kristallogr.* **2005**, *220*, 351–363.
(47) Balzani, V.; Credi, A.; Venturi, M. *Molecular Devices and Machines—A Journey in the Nano World*; Wiley-VCH: Weinheim, 2003.
(48) Sauvage, J. P. *Molecular Machines and Motors*; Structure and Bonding *99*; Springer: Berlin/Heidelberg, 2001.
(49) Browne, W. R.; Feringa, B. L. *Nat. Nanotech.* **2006**, *1*, 25–35.
(50) Kohne, B.; Praefcke, K.; Mann, G. *Chimia* **1988**, *42*, 139–141.
(51) Garcia-Garibay, M. A. *Angew. Chem., Int. Ed.* **2007**, *46*, 8945–8947.
(52) (a) Reddy, C. M.; Gundakaram, R. C.; Basavoju, S.; Kirchner, M. T.; Padmanabhan, K. A.; Desiraju, G. R. *Chem. Commun.* **2005**, 3945–3947. (b) Reddy, C. M.; Kirchner, M. T.; Gundakaram, R. C.; Padmanabhan, K. A.; Desiraju, G. R. *Chem.—Eur. J.* **2006**, *12*, 2222–2234. (c) Reddy, C. M.; Basavoju, S.; Desiraju, G. R. *Chem. Commun.* **2005**, 2439–2441. (d) Reddy, C. M.; Krishna, G. R.; Ghosh, S. *CrystEngComm* **2010**, *12*, 2296–2314.
(53) Mnyukh, Yu. V. *J. Cryst. Growth.* **1977**, *38*, 284–291.
(54) Mnyukh, Yu. V. *Mol. Cryst. Liq. Cryst.* **1979**, *52*, 467–503.
(55) Kitaigorodskii, A. I. *Adv. Struct. Res. Diffr. Methods* **1970**, *3*, 173–247.
(56) Dunitz, J. D.; Bernstein, J. *Acc. Chem. Res.* **1995**, *28*, 193–200.
(57) *Phase Transformations in Solids*; Smoluchowski, R., Mayer, J. E., Weyl, W. A., Eds.; Wiley: New York, 1951.

Chart 1. Chemical Structure of Oxitropium Bromide (OXTB), with the Atom and Bond Labeling Schemes

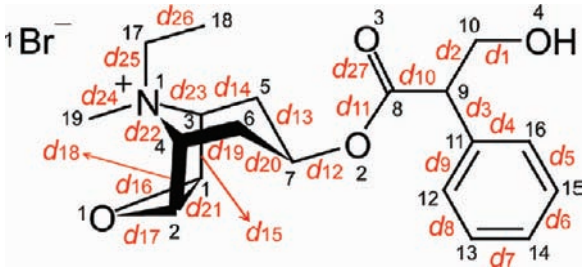

Some of the best known examples of the thermosalient effect are those observed for some inositol crystals, in particular 3,4-di-*O*-acetyl-1,2,5,6-tetra-*O*-benzyl-*myo*-inositol.[9,11,50,58] The transition between phases II and III (according to the original notation)[11] is accompanied by vigorous mechanical motions of the crystals, which are associated with strong contraction of the unit cell along *c* (≈ −12%) and expansion along *a* (+12%) and *b* (+2%), with overall volume expansion of +2.0%. The attempts to explain the origin and mechanism of the thermosalient effect of this compound, however, have remained unsuccessful.

An extraordinary example was observed with *trans*,*trans*, *anti*,*trans*,*trans*-perhydropyrene.[10,50] Upon heating, this solid undergoes a phase transition at 344.5 K, whereupon the crystals jump, having been reported to reach heights of almost 6 cm. Although the rapid sublimation of the high-temperature phase prevented its further analysis, it has been suggested that the transformation is of the martensitic type.[10] An additional example of a thermosalient effect was reported[13] for crystals of 4,5-bis(fluorodinitromethyl)-2-methoxy-l,3-dioxolane, again without elucidation of the structural basis due to the instability of the high-temperature form. Similar problems were encountered during the study of 1,2,4,5-tetrabromobenzene.[15,59,60] The phase transition between the β and γ phases is accompanied by hopping of the crystals to heights of several times their own length and results in disintegration of the starting crystals into smaller, twinned fragments.

Results of our 1994 preliminary study[7] of the thermosalient effect in oxitropium bromide (OXTB, Chart 1) are included in Table 1. Upon heating, OXTB crystals exhibit an endothermic phase transition from form A (OXTB-A) to form B (OXTB-B) (according to the original notation,[7] form I to form II, respectively). The crystal structure of OXTB-A had been determined, while only the cell constants of OXTB-B, refined from the powder X-ray diffraction (XRD) data, were reported in the earlier publication. The transition OXTB-A → OXTB-B, occurring at 331.0 K, is accompanied by a highly anisotropic expansion by 4% of the cell, in which the *b* axis increases by 11% and the *c* axis decreases by 7%. The phase transition is reversible and shows thermal hysteresis, the OXTB-B → OXTB-A transition occurring at 308.2 K (DSC). In 1994, no attempt was made to suggest a mechanism underlying the thermosalient effect in this compound, due to the lack of a crystal structure determination for OXTB-B. We report here the application of additional physical and analytical techniques, along with subsequent data obtained with the earlier applied methods. In addition to providing details on the crystal chemistry of the compound in general, these data afford a basis for understanding the differences between the crystal packing of the two forms and for proposing a mechanism responsible for the thermosalient effect in this system. In addition, we report newly developed techniques for obtaining OXTB-B stable to conversion even at room temperature, as well as two additional solid-state phenomena encountered in the course of the investigation and characterization of this dimorphic system with rich solid-state chemistry.

2. Results and Discussion

2.1. Polymorphism. The crystals used in the 1994 study[7] were obtained by slow evaporation from a 1:1 ethanol:water solution. For the current study, a crystal form screen was carried out by recrystallizing commercial OXTB by slow evaporation from a variety of organic solvents and solvent mixtures of different polarity. The compound crystallized in three different habits comprising two crystalline phases (Figure 1): equidimensional tabular (i.e., blocky) crystals, which resembled those of the commercial sample, were obtained from dichloromethane or from an acetonitrile/dichloromethane mixture, prismatic crystals were obtained from a methanol/dichloromethane mixture, and a second type of prismatic crystals were obtained from dichloromethane, acetone, or chloroform solutions. Single crystals of all three habits, which were stable in air at room temperature, were subjected to single-crystal XRD analysis. Comparison of the cell parameters (Table 1) with those from the crystal structure determination confirmed that the blocky crystals (obtained from dichloromethane and acetonitrile/dichloromethane mixture) and the prismatic crystals obtained from a combination methanol/dichloromethane were internally identical phases (see discussion below) and identical to the commercial sample. This phase, OXTB-A, corresponds to the low-temperature phase I reported earlier[7] and is identical to the structure for which the fractional atomic coordinates had been deposited as a private communication by Schollmeyer and Henk in the Cambridge Structural Database (CALQOW, CCDC no. 185580).[61] We confirmed by single-crystal XRD that the structure of the commercial sample was also identical with this phase. To our surprise, however, the cell parameters of the second type of prismatic crystals, which were obtained from dichloromethane, acetone, or chloroform by slow evaporation at room temperature, were significantly different from those of phase A, but they were essentially identical to those reported for OXTB-B (phase II in the earlier report) based on powder XRD.[7] The identity of this phase, in our hands stable at room temperature, was confirmed by the comparison of the powder XRD pattern simulated from the current single-crystal data with those reported[7] for the high-temperature phase obtained by heating (Figure 2). Both phases are orthorhombic, space group $P2_12_12_1$, differing significantly in the *b* and *c* cell axes, which is reflected as a difference in the cell volumes of about 80 Å^3 (Table 1). There is no evidence that the OXTB-B crystals obtained in this manner spontaneously convert at room temperature to the OXTB-A phase.

2.2. Thermosalient Effect (Jumping Crystals). 2.2.1. Differential Scanning Calorimetry (DSC). Our earlier experiments[7] indicated a variability of thermal behavior of single crystalline samples with morphology. To check if the thermal behavior of the crystals of phase A is a function of crystal habit, very

(58) Fattah, J.; Twyman, J. M.; Dobson, C. M. *Magn. Reson. Chem.* **1992**, *30*, 606–615.
(59) Gafner, G. *Acta Crystallogr.* **1960**, *13*, 706–716.
(60) Gafner, G. *Acta Crystallogr.* **1964**, *17*, 982–985.
(61) Allen, F. H. *Acta Crystallogr.* **2002**, *B58*, 380–388.

Table 1. Comparison of the Unit Cell Parameters of the Two Phases of Oxitropium Bromide Prepared by Different Methods

phase	origin/reference	*a*, *b*, *c*/Å	*V*/Å^3
	Literature Data		
OXTB-A	CSD[a]	7.3914(4), 10.1215(6), 24.690(1)	1847.1
OXTB-A (296 K)	Bernstein et al.[b,c]	7.388(2), 10.118(3), 24.705(4)	1846.7
OXTB-A (327 K)	Zamir[d]	7.410(2), 10.18 (2), 24.63(3)	1849
OXTB-B (331 K)	Zamir[d]; Bernstein et al.[b,e]	7.477(2), 11.25(2), 22.86(6)	1925
	This Work		
OXTB-A (blocky)	recrystallization[f]	7.3861(2), 10.1229(2), 24.6403(4)	1842.3
OXTB-A (prismatic)	recrystallization[g]	7.3927(2), 10.1512(4), 24.6291(9)	1848.3
OXTB-B	recrystallization[h]	7.4514(2), 11.2179(3), 22.8043(6)	1906.2
OXTB-B	heating of OXTB-A	7.453(2), 11.220(4), 22.790(7)	1905.8
OXTB-B	UV irradiation of OXTB-A[i]	7.4709(7), 11.228(1), 22.798(2)	1912.3

[a] The basic unit cell parameters and the fractional atomic coordinates were deposited in the Cambridge Structure Database in 2002 by D. Schollmeyer and M. Henk as a private commmunication (CALQOW, CCDC no. 185580). [b] Zamir, S.; Bernstein, J.; Greenwood, D. J. *Mol. Cryst. Liq. Cryst.* **1994**, *242*, 193−200. [c] Single-crystal XRD data obtained from a sample crystallized from 1:1 ethanol:water mixture. [d] Zamir, S. Ph.D. Thesis, Ben-Gurion University of the Negev, Beer Sheva, Israel, 1995. [e] Powder XRD data from a sample obtained by heating. [f] Blocky crystal obtained from dichloromethane. [g] The cell parameters of the prismatic habit obtained from methanol were identical within experimental error. [h] Solvent: dichloromethane. [i] Source: 250 W medium-pressure Hg lamp.

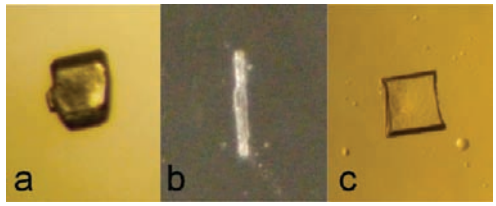

Figure 1. Three different habits of OXTB obtained by recrystallization of the commercial sample at room temperature: blocky (a) and prismatic (b) crystal of phase OXTB-A, and a crystal of phase OXTB-B (c). The largest size of the crystals shown here was 0.3−0.5 mm.

accurate DSC measurements were performed below the melting temperature on pure bulk samples of blocky and prismatic crystals of OXTB-A, as well as on the commercial (as-obtained) sample, which was composed of blocky crystals. The reproducibility of the phase transition temperatures was examined by multiple heating/cooling cycles.

On heating, the prismatic crystals of OXTB-A exhibited a single endothermic peak corresponding to the phase transition to OXTB-B at 318 K (Figure 3a). Cooling of that sample led to exothermic conversion back to OXTB-A, with a single peak at 300 K, corresponding to a hysteresis of 18 K. In the second and all subsequent cycles, the sample behaved in an identical way, and no changes in the phase transition temperatures or the shapes of the DSC peaks were observed.

On the other hand, despite the fact that they have identical crystal structures (see the discussion of the XRD results below), the blocky crystals of OXTB-A (Figure 3b) and the crystals of the as-obtained sample (Figure 3c) exhibited somewhat different thermal behavior relative to the prismatic crystals. During the first heating, the DSC curves exhibited *two* overlapped but clearly distinguishable peaks, the first one at 316 K for the blocky crystals and 317 K for the as-obtained sample, and the second one at 319 K for both samples (see the insets in Figure 3b,c). On cooling, a single exothermic peak corresponding to the OXTB-B → OXTB-A conversion appeared in both cases, at 300 K for the blocky crystals and at 299 K for the as-obtained sample. Notably, subsequent to the first cycle, these two samples behaved in an identical way to the prismatic crystals; i.e., the forward (A → B) and the reverse (B → A) phase transitions appeared as single peaks.

The variation in the thermal behavior of different crystal habits of OXTB-A prompted investigation of the effect of aging of the blocky crystals. After two thermal cycles, the blocky

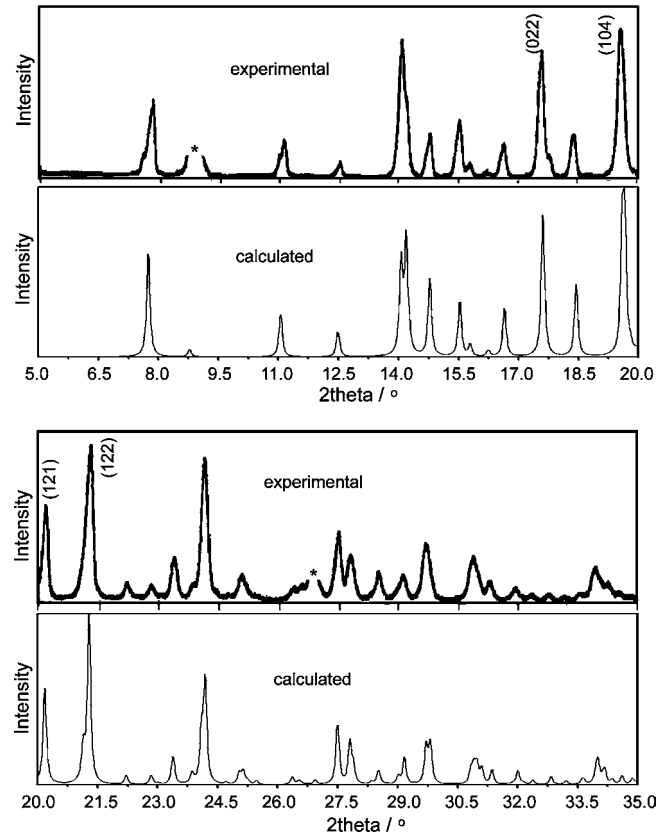

Figure 2. Experimental[7] and calculated X-ray powder diffraction patterns of the high-temperature form (OXTB-B) of oxitropium bromide (λ = 1.54056 Å). The asterisks denote regions where peaks from the standard (fluorophlogopite) appear.

crystals of OXTB-A behaved in an identical way to the prismatic crystals following the first heating cycle and were then left in the calorimeter overnight, under atmospheric conditions. The original behavior of this sample was partially recovered; the temperature of the A → B transition increased from 316 to 317 K, indicating that the original state of the sample had been partially restored. As with the original sample, in the subsequent cycles (fourth and fifth) the sample behaved as the prismatic crystals, showing that the effect was reproducible. The aging did not affect the B → A transition at 299 K. These results confirm our previous observations[7] that the exact temperature of the phase transition A → B depends on the history of the

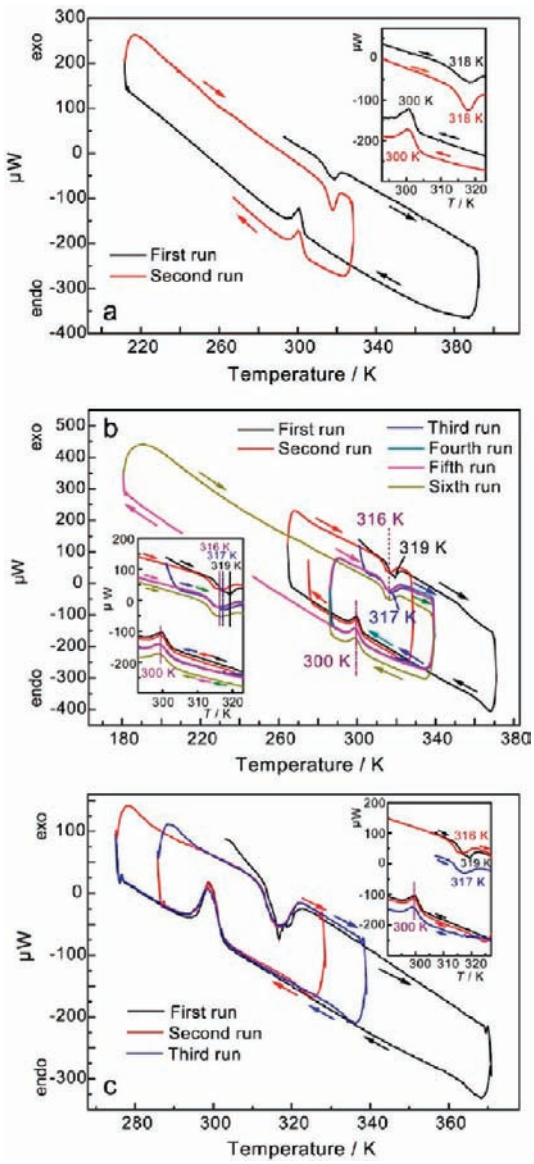

Figure 3. DSC curves of the *prismatic* crystals (a), the *blocky* crystals (b), and the commercial sample (c) of OXTB-A. The arrows indicate the direction of the temperature change. Heating/cooling rate: 5 K·min^{-1}. The third run in panel b was recorded after the sample had stood overnight at room temperature.

OXTB-A sample. These observations suggest that block-shaped crystals of OXTB-A do not change directly to phase B; instead, they appear to go through a transition stage, involving a phase which is energetically quasi-degenerate with phase A.

2.2.2. Characterization of the Single-Crystal-to-Single-Crystal Phase Transition. In the course of undergoing a vigorous thermosalient effect (usually around 328−329 K; see Movie S1 in the Supporting Information), if the crystals of OXTB-A are not attached to the basis, they can jump several centimeters! Although rapid heating (10 K·min^{-1}) usually results in disaggregation of the crystals, we found that slower heating (4−5 K·min^{-1}) results in a smooth single-crystal-to-single-transition as observed on the hot-stage microscope (see Movie S2 in the Supporting Information). Under such conditions, the physical integrity of the single crystal and its ability to diffract X-rays were completely preserved. The single-crystal-to-single-crystal transition was verified by single-crystal oscillation (Figure 4) and Weissenberg (Figure S1, Supporting Information) photography about the *b* axis. The oscillation photo at room temperature (Figure 4a) exhibited a layer line spacing equivalent to an axis of 10.16 Å. Heating the crystal to 331.8 K reduced the layer line spacing in the oscillation photo (Figure 4b) by 4.4 mm, corresponding to an increase of the *b* axis to 11.15 Å.

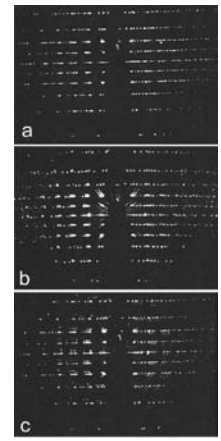

Figure 4. Oscillation photographs recorded by oscillation of a single crystal of oxitropium bromide about the *b* axis at room temperature (a), after the phase transition (b), and at room temperature (c).

2.2.3. Direct Structural Evidence for the Mechanism from Single-Crystal X-ray Diffraction. The OXTB-A → OXTB-B transition induced by slow heating was monitored by single-crystal X-ray structure determinations.[62] The diffraction data of OXTB-B, which was obtained by heating a crystal of OXTB-A above 293 K, were collected at 301−302 K, (i.e., 1−2 K above the transition temperature of OXTB-B → OXTB-A, 300 K). This temperature was sufficient to prevent the reverse phase transition, while it provided conditions closest to those used for structure determination of OXTB-A, as well as minimum possible thermal effects on the structure of OXTB-B. The structure analysis confirmed that the thermally obtained OXTB-B was identical to that obtained by recrystallization at room temperature.

The crystallographic data and refinement details are given in Table S1 in the Supporting Information. Both phases are orthorhombic, space group $P2_12_12_1$, with $Z' = 1$. Generally, the molecular structures of OXTB in the two phases (Figure 5) appear similar, but unlike OXTB-A, the enlarged atomic thermal motions in the phenyl ring in OXTB-B are significantly increased, suggesting the possibility of disorder. However, the pattern of enlargement of the thermal ellipsoids suggests that the phenyl group is undergoing a rigid-body motion that can be described as wagging about the *ipso*-carbon atom.

The differences in crystallographic metrics (cell constants and molecular geometry) qualitatively do not appear to be particularly striking in view of the rather dramatic physical manifestation of the A → B phase change. Nevertheless, they provide a gauge or a benchmark for the magnitudes of the concomitant microscopic geometric perturbations associated with the significant physical macroscopic manifestation of those alterations.

The *molecular conformations* for the starting and final states are readily compared by the overlap of the stick diagram. The three bridging atoms (O2, C8, and C9 in Chart 1) and the rigid

(62) Our first report[7] contains complete information on the earlier structure determination of both forms, but the details on form B were not generally available. Hence, after a hiatus of 15 years, the crystal structures of the two forms were independently redetermined with virtually identical results.

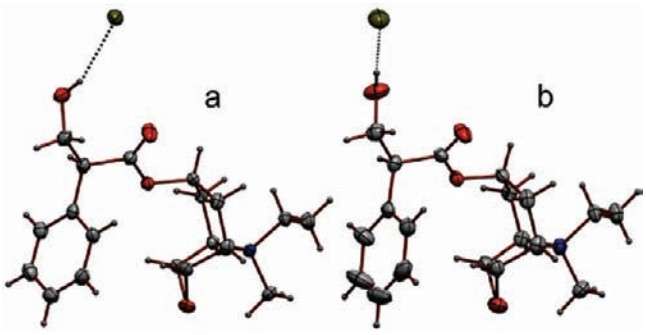

Figure 5. ORTEP-style representation of the molecular structures (plotted at 30% probability level) of phase A (a) and phase B (b) of oxitropium bromide.

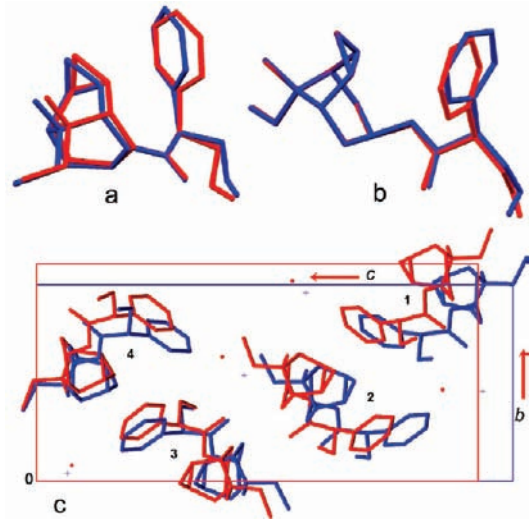

Figure 6. Stick-type representations of the structures of phase A (OXTB-A, blue) and phase B (OXTB-B, red) overlapped at the three bridging atoms (a), at the tricyclic moiety (b), and at the cell origin (c). Regarding the hydrogen atoms, only that of the hydroxyl group is shown in plots a and b. Plot c depicts the changes of the cell size and the changes in molecular disposition induced by the phase transition.

tricyclic system were each overlapped by a least-squares procedure; the resulting overlap diagrams are presented in Figure 6. Table S2 in the Supporting Information summarizes the largest quantitative geometrical differences between the molecules of OXTB-A and OXTB-B (distances that differ by >1%, angles that differ by >1°, and dihedral angles that differ by >3°; a complete list of intramolecular parameters is deposited in the Supporting Information as Tables S4−S7). As expected from energetic considerations,[63] the bond distances in the two phases are very similar. The overlapped models in Figure 6 clearly show that, while the geometry of the epoxy-aza-tricyclic-nonyl portion of the molecule is rigid and remains essentially unchanged, the molecule is flexible at the ester linkage (O2), the carbonyl group (C8), and the connection between the phenyl ring and the hydroxymethyl group (C9). The flexibility at the ester bridge results in conformational differences between the two phases, which are manifested as different orientations of the two terminal groups relative to the molecular backbone: the phenyl ring and the hydroxyl functionality. The dihedral angle of the phenyl ring relative to the bridge (O2−C8−C9) changes by ~8°, from 80.6(2)° in OXTB-A to 88.9(3)° in OXTB-B. Accordingly, the largest differences in the angles were observed around the bridging atoms C8 and C9 (labels refer to Chart 1): the angles d_1-d_2, $d_{10}-d_3$, and d_3-d_2 differ by 4.9(6), 3.8(6), and 2.9(6)°, respectively, while the dihedral angles $d_{27}-d_{10}-d_2$, $d_{27}-d_{10}-d_3$, $d_{10}-d_3-d_9$, and $d_2-d_3-d_9$ differ by as much as 15.7(1.0), 14.7(8), 15.1(7), and 16.0(8)°, respectively.

The question of similarity or difference between the two *crystal structures* can be examined by comparing a profile of the surroundings of a single molecule, as represented by the Hirshfeld surfaces[64−68] of the OXTB molecule in the two phases (Figure 7). The differences in the Hirshfeld fingerprint images for the two structures are readily distinguishable, clearly indicating a different molecular environment in the two structures and the rather high sensitivity of this method for the comparison of polymorphic structures.

In both phases, the hydroxyl group O4H is hydrogen-bonded to the bromide ion, with very small difference in the hydrogen bond distance: d(O4···Br1) = 3.260(2) and 3.221(3) Å in OXTB-A and OXTB-B, respectively. The slightly shorter hydrogen bond in OXTB-B is accompanied by a larger O4−H4···Br1 angle, 170.8°, relative to 156.7° in OXTB-A. Inspection of the crystal packing (Figure 6c) shows that the conformational changes of the oxitropium cation are accompanied by the less-dense packing of OXTB-B relative to OXTB-A, which is also reflected in the calculated density values (1.437 and 1.482 g·cm^{-3}, respectively). The phase change OXTB-A → OXTB-B is accompanied by an expansion of nearly 10% along the *b* axis, from 10.1512(4) to 11.2179(3) Å, and shrinkage of 8% along the *c* axis, from 24.6291(9) to 22.8043(6) Å, resulting in the net cell volume expansion of 4%. The cell expansion leads to an increase in the separation between two ions of the same charge, while the distance between a cation and the nearest anion changes considerably less. For instance, the distance between atoms C9 of the molecules labeled in Figure 6c with **1** ($-^1/_2 + x$, $1.5 - y$, $2 - z$) and **2** ($1.5 - x$, $1 - y$, $-^1/_2 + z$) increases from 6.951 Å in OXTB-A to 7.458 Å in OXTB-B, while that between the respective C7 atoms increases from 9.927 to 10.076 Å. The distance between the respective bromide ions changes from 11.633 to 10.721 Å. If molecules **2** ($1.5 - x$, $1 - y$, $-^1/_2 + z$) and **3** ($2 - x$, $-^1/_2 + y$, $1.5 - z$) in Figure 6c are considered, the distance between the C9 atoms decreases from 10.184 to 8.933 Å, and that between the C7 atoms decreases from 6.092 to 6.068 Å. The distance between the respective bromide ions increases from 15.193 to 16.014 Å.

2.2.4. Analysis of Atomic Displacement Parameters and the Driving Force of the Phase Transition. The atomic displacement parameters (ADPs) describe the time and space average of movements of atoms in the crystal—the so-called thermal motion—and hence are often referred to as temperature factors. Comparison of the ADPs of OXTB-A at 300 K with those of OXTB-A at 327 K can provide information to determine preferential directional motions for the molecules in the course of the phase trasition. That pattern of preferential directions may

(63) Bernstein, J. *Polymorphism in Molecular Crystals*; Oxford University Press: Oxford, 2002; p 94.

(64) Hirshfeld, F. L. *Theor. Chim. Acta* **1977**, *44*, 129–138.
(65) McKinnon, J. J.; Spackman, M. A. *Chem. Commun.* **2007**, 3814–3816.
(66) McKinnon, J. J.; Mitchell, A. S.; Spackman, M. A. *Chem.—Eur. J.* **1998**, *4*, 2136–2141.
(67) McKinnon, J. J.; Spackman, M. A.; Mitchell, A. S. *Acta Crystallogr.* **2004**, *B60*, 627–668.
(68) Wolff, S. K.; Grimwood, D. J.; McKinnon, J. J.; Jayatilaka, D.; Spackman, M. A. *Crystal Explorer*; University of Western Australia: Perth, Australia, 2007.

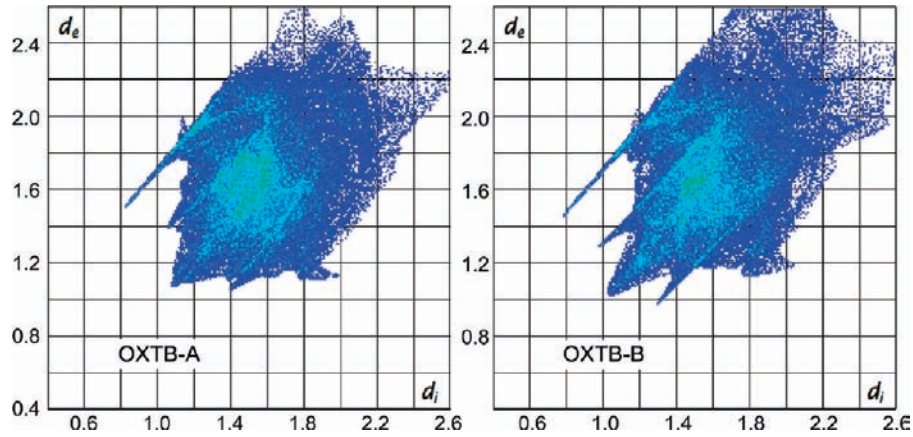

Figure 7. Fingerprint plots of the Hirshfeld surfaces[64−68] of the two OXTB phases.

be looked upon as representing vectors along the reaction coordinate of the molecule in the course of the phase change and can be visualized by calculating and plotting the *differences* in the ADPs at the two temperatures using a method developed by Bürgi et al.[69]

First, the ADPs for each structure were analyzed by the Trueblood−Schoemaker (TS) method[70] to determine if the cations behave as rigid bodies, which is a necessary condition for the subsequent analysis. In this case the TS method assumes that the entire molecule is a rigid body and then carries out a least-squares fit between that rigid body and the experimentally determined ADPs for the motion of the whole rigid-body motion (expressed as translations, librations, and screw motions) to test the validity of the model; for both phases the rigid-body model was validated. Then, to obtain a graphical representation of the differences in the ADPs, it was necessary to superimpose the two cationic molecular structures, which was accomplished by determining the best least-squares fit[71] between the molecules in the two crystal structure determinations with the aid of the TRANS software.[69] The output was then used with the PEANUT program[72] to calculate the graphical representation of the differences in ADPs between the two structures.[73]

Figure 8 presents the PEANUT diagram of the difference of the ORTEPs, drawn at the 50% probability level, for the two structure determinations of OXTB-A at 300 and 327 K.[7] It is possible to recognize visually some differences in the ADPs of the following atoms: O3, some of the phenyl carbon atoms, C17, C18, C19, and the epoxide oxygen O1. In Figure 8, the solid lines represent positive differences and the broken lines represent negative differences in the ADPs of form A between 300 and

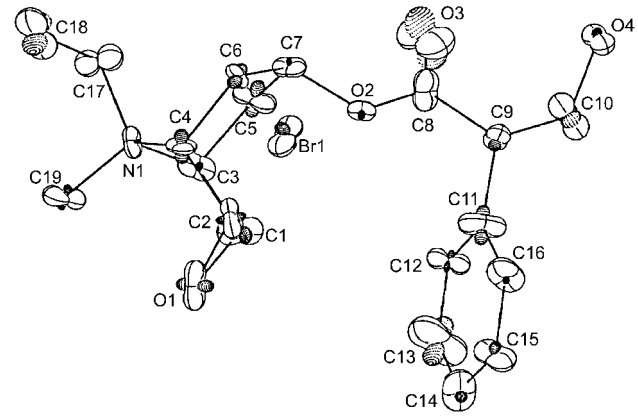

Figure 8. PEANUT diagram representing the differences in ADPs for the structure determinations of OXTB-A at 300 and 327 K (the original ORTEPs were calculated at the 50% probability level). Regions of positive difference are unfilled and represent the increase in thermal motion with temperature, hence increased motion along the reaction coordinate defined by the direction of the lobes. Shaded regions are negative differences.

327 K. There is a clear indication of the changes in amplitude *and* direction in the atomic motion with heating. Since the phase change does take place slightly above 327 K, the structures at these two lower temperatures must lie on the multidimensional reaction coordinate for the transition. Two interpretations may be suggested for these changes: (a) the changes in the direction of the vibrational movement indicate the incipient geometric change which the molecule will undergo during the transition; (b) since the crystal structure represents time and space averages over the entire crystal, the diagram already represents the individual molecules (or collections of molecules) that have undergone the conformational change that all the molecules will eventually undergo. However, the second interpretation does not provide a rationale for the mechanical macroscopic perturbation concomitant with the observed phase change; on the other hand, additional experimental *proof* for the first interpretation is also lacking. The observation of the abrupt thermosalient effect argues in favor of the first interpretation, namely, that the molecules acquire sufficient vibrational energy in the directions indicated to overcome the barrier indicated by the directional properties of the PEANUT diagram—that is, in the direction of positive difference in ADPs.

2.2.5. Mechanical Aspects of the Phase Transition. We noted earlier that the internal structural phase change is anisotropic and that the crystals apparently jump in two directions. It was

(69) (a) Hummel, W.; Hauser, J.; Bürgi, H.-B. *J. Mol. Graphics* **1990**, *8*, 214–220. (b) Hummel, W.; Rasell, A.; Bürgi, H.-B. *Acta Crystallogr.* **1990**, *B46*, 683–692.
(70) Schomaker, V.; Trueblood, K. N. *Acta Crystallogr.* **1968**, *B24*, 63–76.
(71) McLachlan, A. D. *J. Mol. Biol.* **1979**, *128*, 49–79.
(72) Baram, J. Ph.D. Thesis, Ben-Gurion University of the Negev, 1980.
(73) Briefly, the PEANUT program works as follows. The tensor **U** that describes the mean square displacement (MSD) of the atoms can be represented in a number of ways: (a) as the second order ellipsoidal surface, as is commonly presented in ORTEP (Oak Ridge Thermal Ellipsoid Plotting) plots, or (b) as a surface of an ovaloid which is a sixth-order surface that can represent the MSD. The square root of the MSD (RMSD) can be represented by a quartic surface. The PEANUT program was written to calculate and graphically present the *differences* between surfaces (e.g., ORTEP surfaces) of two determinations of the same molecular structure, for instance, between a theoretical calculation and an experimental one, or as in the present case for structures determined at different temperatures.

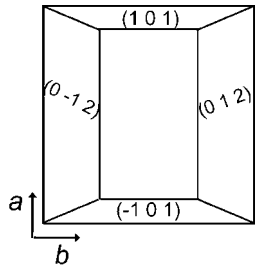

Figure 9. Schematic diagram of the habit of crystals used to study the jumping phenomenon, shown with the face indexes. The main face in the center is (001).

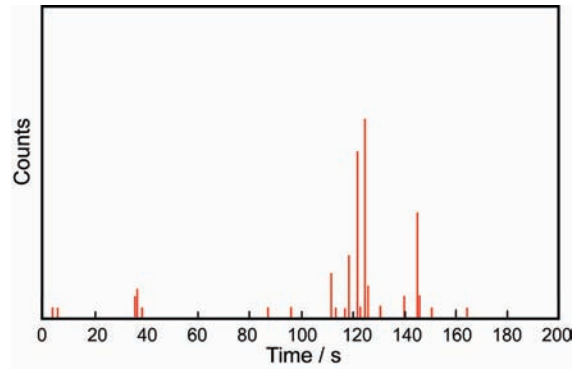

Figure 10. Acoustic emission from oxitropium bromide crystal as a function of time. In this case, the phase transition occurred after ~120 s, with a large acoustic response.

of interest to determine if the direction and the height of the jumping were dependent upon the initial orientation of the crystals on the hot stage, and if these effects were further dependent on the rate of heating and cooling. To examine the possible role of these parameters, photographs of dozens of crystals were examined under the microscope to determine the face on which they were lying, and their subsequent behavior during heating on the hot stage was followed by video photography. The following observations were made:

(a) The height of the jumping ranged from 0 to about 2 cm.
(b) Some crystals did not jump during heating; they simply expanded.
(c) There was no apparent connection between the direction of the jumping and the initial orientation of the crystal. Because of the crystal habit, naturally most of the crystals tended to lie on the largest face, (001) (Figure 9), that is, parallel to the crystal axis of expansion (*b*), but in any case they jumped up rather than sideways.
(d) As pointed out earlier, in order to obtain high-quality crystals of OXTB-B resulting from the single-crystal-to-single-crystal phase transition, a slow heating rate (≤ 5 $K \cdot min^{-1}$) is necessary. A more rapid heating rate results in the explosion of many of the crystals in the course (or as a result) of the phase transformation and the jumping, but the heating rate apparently is not a factor determining the height of jumping.
(e) The height of jumping during the cooling cycle was generally smaller than that during the heating cycle, although the reduced quality of the crystals resulting from the previous heating cycle precluded quantification of this result.
(f) Following a heating and cooling cycle, crystals generally maintained physical integrity, but microscopic examination revealed that the initially transparent crystals became opaque, accompanied by the formation of a large number of cracks.

These phenomena contain many elements of martensitic phase transformations in metals which are characterized by cooperative, homogeneous movements resulting in a change in the crystal structure:[72,74] (a) many atoms undergo movement at one and the same time, in identical movements over distances that are small compared to the lattice constants; (b) the transformation is an imposed process, accompanied by a change in volume and a change in the morphology of the surface; (c) the neighbors of every atom are conserved; (d) the transformation is reversible; and (e) the transformation takes place with nucleation and growth. While this description refers generally to phase changes in metals, there are a number of features that may be applied to the molecular system under study: the change in volume, the change in the surface morphology, the reversibility of the process, the occurrence of nucleation and growth processes, and the small change in structure (that is, no breaking and/or making of chemical bonds). Yet, the above description is not entirely suitable for this system, since all the atoms apparently do not move simultaneously and together in this process, clearly a result of the fact that this system involves a *molecular* (ionic) instead of a metallic crystal, the latter being comprised of individual atoms. In this case, the definition must describe the movement of whole molecules rather than atoms.

Because a martensitic transformation involves the movement of a large number of atoms/molecules (and thus results in formation of fractures and strains in the crystal), it should be accompanied by the formation of an elastic wave in the material. The acoustic emission during the course of the phase change can be measured experimentally (the acoustic emission, also known as stress wave emission, is a transitory elastic wave which is formed by the rapid release of energy from the material[75]), and the detection of this emission is expected to prove the existence of mechanical stresses and strains in the crystal undergoing the phase change, consistent with the martensitic transition.

To measure the acoustic response, a crystal of OXTB was placed between two copper plates (no glue was used) and heated. Acoustic signals were detected, and in the course of the transformation the crystal disintegrated to a rough powder. Cooling subsequent to the phase transition yielded a more finely divided powder; that is, all the larger crystallites resulting from the disintegration during the first heating cycle were transformed to smaller microcrystals.

The graph showing the intensity of the acoustic emission as a function of heating time is shown in Figure 10. The high-intensity emission occurs 120 s following the onset of heating and provides evidence for the occurrence of acoustic waves during the phase transition. For single crystals that did not suffer disintegration in the course of the phase change, it was possible to visually detect the anisotropic manifestions of the movement in a specific direction in the crystal with scanning electron microscopy (SEM). An image of such a crystal is shown in Figure 11.

It is possible to estimate the number of molecules in the crystal with a particular mass (*m*) that must undergo a

(74) Porter, D. A.; Easterling, K. E. *Phase transformations in metals and alloys*; Chapman & Hall: London, 1992.

(75) American Society for Testing and Materials. Acoustic Emission Working Group Subcommittee Report. Report ASTM-STP-505, 1972.

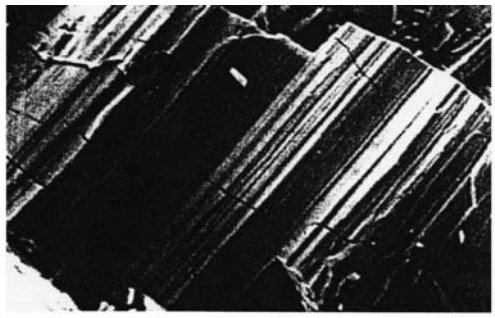

Figure 11. SEM image of an OXTB crystal following the phase transformation to the high-temperature phase. The anisotropic emergence of a fracture plane from the crystal surface is clearly visible as sharp white streaks.

simultaneous conformational change in order to enable the crystal to reach the height h, with the accompanying change in potential energy. The calculation assumes that the thermal energy is due to a single degree of freedom in the molecule at temperature T. For a crystal of mass m jumping to a height h, the following parameters were used: $m = 1 \times 10^{-4}$ g, $h = 1$ cm, $T = 330$ K. According to a comparison of the potential energy of the crystal when it reaches a height of 1 cm ($mgh \cong 0.1$ erg) with the amount of energy associated with one molecular degree of freedom, 4.5×10^{-14} erg, the number of molecules, N, that must undergo the conformational change to bring about the jumping is

$$N = \frac{(1 \times 10^{-14}\ \text{g})(6 \times 10^{23}\ \text{mol}^{-1})}{412\ \text{g}\cdot\text{mol}^{-1}} = 10^{17}\ \text{molecules}$$

Then,

$$n = \frac{0.1\ \text{erg}}{4.5 \times 10^{-14}\ \text{erg}} = 10^{12}\ \text{molecules}$$

The fraction of molecules in the crystal that must undergo a change in geometry that will result in a jumping crystal is

$$n/N = 10^{-5}$$

Since we have seen that there is acoustic emission from the crystal, it is possible to estimate the time required for transformation from the speed of sound in that time. The speed of sound in solids is in the range 500−13 000 $\text{m}\cdot\text{s}^{-1}$.[76] Based on the assumption that the speed in this case was of the order of 10^5 $\text{cm}\cdot\text{s}^{-1}$, and assuming a crystal size on the order of 0.1 mm in each dimension, the duration of the phase transition is approximately 10^{-7} s.

This calculation can be used to compare the mechanical energy of the jumping with the thermal energy that is acquired by the crystal taking account of the molecular degrees of freedom. Of course, a flexible molecule such as OXTB naturally has many more than one degree of freedom, and inclusion of a greater number will decrease the fraction of molecules from the above number. As described above, a possible mechanism to explain the jumping phenomenon is comprised of two steps. The first involves the change in conformation of a number of molecules from one conformational local energy minimum to another and results in a packing arrangement that does not stabilize that conformation, resulting in the generation of mechanical strain, as in the compression of a spring. The second step is a simultaneous or concomitant process involving decompression of the "spring", which is released by the crystal jumping, accompanied by a relaxation of the molecules to a conformation similar to that observed at low temperature. This mechanism is somewhat complicated, but it does incorporate all of the observations and the calculations already noted: the existence of additional molecular conformations in the local energy minima, the directional properties of the changes in the anisotropic thermal parameters prior to the phase change, the generation of an acoustic wave during the transformation (which provides evidence for the release of mechanical tension built up in the crystal), and the fact that the molecular conformation in OXTB-A is very similar to that in OXTB-B, despite the fact that significant mechanical changes take place in the macroscopic crystal.

2.3. Infrared Spectroscopy and UV-Induced Reactions. Since we were interested in the possible photosensitivity of OXTB, we also investigated the effect of ultraviolet (UV) radiation on the crystals of OXTB-A. For that purpose, single crystals of OXTB-A were exposed to heat-filtered UV light from a medium-pressure Hg lamp (SP-7 Ushio, 250 W). After exposure to UV light for less than 3 min, single crystals of OXTB-A were completely converted into OXTB-B, with total preservation of the crystallinity. The XRD analysis of the resulting single crystals of OXTB-B (Table S1, Supporting Information) showed that their structure was identical to that of OXTB-B obtained by recrystallization (from acetone and chloroform) and by heating, which is also obvious from the overlapped plot of the molecular structures (see Figures S2 and S3 in the Supporting Information; a detailed comparison of the intramolecular parameters of OXTB-B prepared in different ways is deposited as Tables S4, S5 and S7 in the Supporting Information). The identity of the molecular structures of thermally induced OXTB-B with OXTB-A was confirmed by the similarity of the NMR spectra.

The OXTB-A → OXTB-B phase transition was also characterized by IR spectroscopy. Consistent with the X-ray data, the IR spectra of the blocky and prismatic crystals of OXTB-A were identical, and the spectra of heated and UV-irradiated crystals corresponded to those of OXTB-B (Figure 12). In the process of verifying the reproducibility of these spectra, however, we noticed two spectral peculiarities connected with the sample preparation that strongly influenced the spectral appearance. First, by prolonged grinding of OXTB-A (blocky or prismatic crystals), with or without KBr, the carbonyl stretching band at 1726 cm^{-1} gradually and completely disappeared, with simultaneous evolution of a new band at 1735 cm^{-1} (Figure 13). This indicates that, in addition to heating and UV irradiation, the phase transition of OXTB-A → OXTB-B can be induced by mechanical pressure. In addition, the IR spectrum of the UV-irradiated samples depended on whether the irradiation was carried out in the presence or in the absence of KBr. Specifically, the spectrum of a mixture of OXTB-A and KBr which was irradiated with UV light was different from that of the OXTB-A which was irradiated with UV light and then mixed with KBr to record the spectrum (Figure S4, Supporting Information). Both transformations, induced by grinding and by UV light in the presence of KBr, were completely reproducible. ^{1}H NMR analysis (methanol-d_4) of the samples before and after the treatment showed that, while the grinding or UV

(76) *CRC Handbook of Chemistry and Physics*, 55th ed.; Taylor & Francis: 1972; p , E-47.
(77) Lehmann, O. *Z. Kristallogr.* **1877**, *1*, 97–131.

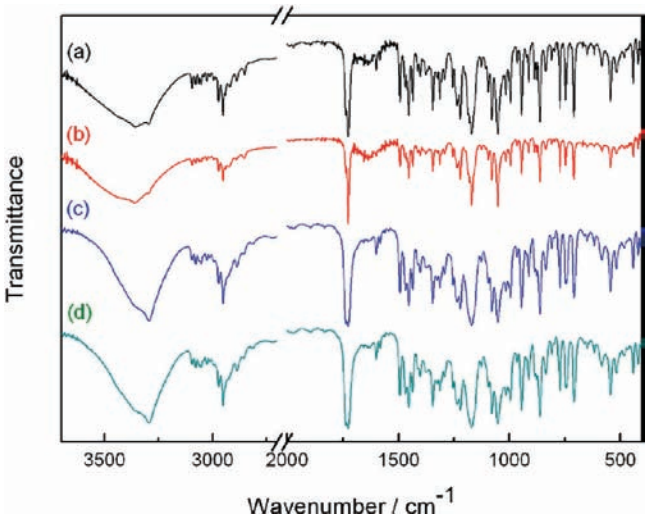

Figure 12. IR spectra of blocky crystals of OXTB-A (a), prismatic crystals of OXTB-A (b), heat-induced OXTB-B (c), and UV-induced OXTB-B (d).

irradiation alone induced the phase transformation of OXTB-A → OXTB-B (no changes in the ^{1}H NMR spectrum after dissolution), UV irradiation of OXTB *mixed with KBr* caused significant, irreversible spectral changes of the extracted material. Detailed analysis and assignment of the NMR spectrum of the product (see Figures S3 and S5, Supporting Information) revealed that, in the presence of KBr, OXTB underwent a UV-induced reaction at the bistricyclic moiety, probably opening of the epoxide ring, while the remaining part of the molecule remained unchanged.

2.4. Heating to Melting Point. Section 2.2.1 summarizes the thermal behavior immediately above and below the temperature of the phase change. In optically following the behavior of single crystals upon heating to the reported[7] melting point (∼478 K) on the microscope hot stage, we noted some unusual behavior. As shown in Figure 14, beginning at 472 K, bubbles start to appear in the bulk of the crystals which have been immersed in silicone or mineral oil. The gas evolves from the surface of all crystal faces, accompanied by a penetrating odor, but the crystals

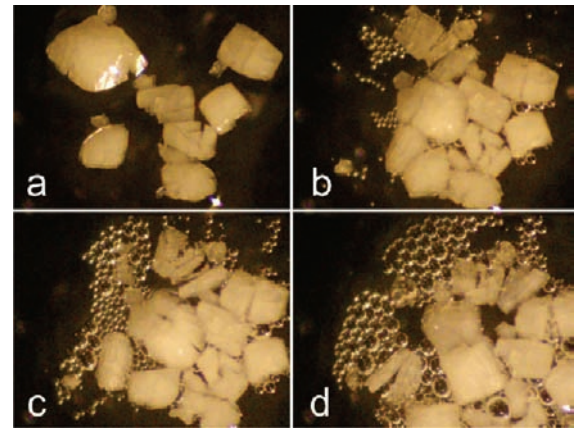

Figure 14. Effect of heating crystals of OXTB close to the melting point. The crystals were immersed in silicone oil to facilitate observing the emanation of gas bubbles: (a) prior to onset of heating; (b) onset of emanation of gas bubbles at ∼473 K; (c) temperature maintained at ∼473 K with increased emanation of bubbles but virtually no deterioration in the physical integrity of the crystals; (d) increased flow of bubbles has agitated the crystals to new positions, but there is still little degradation in physical integrity.

Scheme 1. Mechanism of the Decomposition of Oxitropium Bromide below the Melting Point

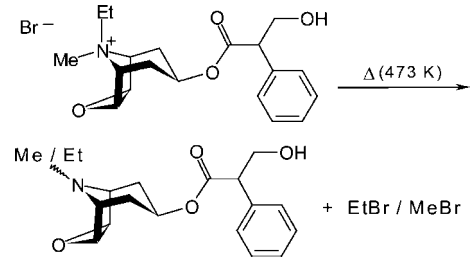

maintain their physical integrity. In view of the nature of the molecular structure of OXTB and the stench of the evolved gas, we suspected that the reaction in Scheme 1 was likely taking place in the solid.

To verify this mechanism, the melt was dissolved in $CDCl_3$ and analyzed by ^{1}H NMR spectroscopy. The *N*-ethyl group was

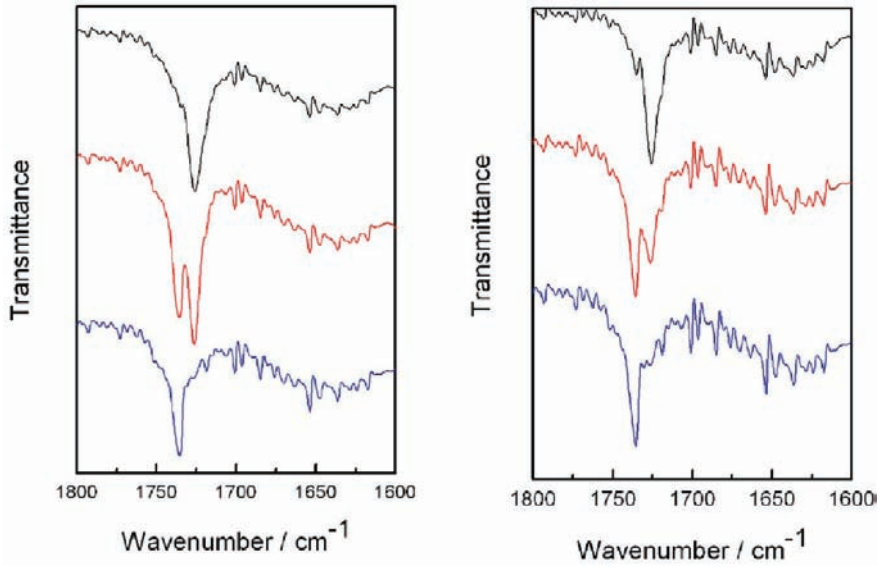

Figure 13. Comparison of the effects of grinding on the spectra of the blocky (left) and prismatic (right) crystals of the phase A of OXTB. The grinding time increases from the top to the bottom plot. The weak band intensity is due to the small amount of the pure phases available.

identified by a quartet at 2.64 ppm ($J = 7.1$ Hz) and a triplet at 0.93 ppm ($J = 7.1$ Hz). Integration of the singlet *N*-methyl proton against the triplet proton of the *N*-ethyl group indicated that the two are present in a 7:3 ratio in the melt, meaning that the gas that evolved from the crystal was composed of ethyl bromide and methyl bromide in the ratio 3:7.

3. Conclusions

A review of the rather limited literature on thermosalient molecular crystals reveals, not surprisingly, that virtually all of the systems reported were discovered serendipitously, in the course of other investigations. Also perhaps not surprisingly, a common feature is that the jumping effect was detected because the crystals were carefully observed—or better still, video-recorded—in the course of a melting point determination on a hot stage. While hot-stage microscopy has been in use at least since 1877,[77] and was widely used into the middle of the 20th century, it had given way to more "numerical" analytical methods. With the development of inexpensive digital photography and recording, combined with the relative ease of publishing photographic images and depositing video recordings, the technique is enjoying a deserved renaissance. As its use becomes more widespread, no doubt more instances of this thermosalient phenomenon will be recorded and studied.

In a study of a rather dramatic and still poorly understood phenomenon such as the thermosalient effect, one of the principal goals is to gain an understanding of the nature and mechanism of the phenomenon. Achieving that goal requires the application of a wide variety of analytical techniques, each of which can provide part of the overall picture. In this case, we have applied microscopy and a variety of thermal, spectroscopic and structural methods to characterize in great detail the nature of the phenomenon and to provide data and information that facilitate the proposal of a mechanism at the molecular structural level for the effect. Although this is one of the most complete studies to date of the thermosalient phenomenon, there are still many questions to be answered. Just as every crystal structure is different, so every thermosalient system will be different and will provide understanding and insight into the phenomenon. These remain fascinating systems from the point of view of their crystal chemistry, but molecular thermosalient systems, especially reversible ones of the type studied here, are of considerable potential use for coupling thermal and mechanical energy at the microscopic level.

4. Experimental Section

4.1. Materials and Preparation Procedure. For experiments initially carried out in Beer Sheva, oxitropium bromide (OXTB) was obtained from Boehringer-Ingelheim (courtesy of Dr. Dan Greenwood). For those in Osaka, it was purchased from the European Directorate for the Quality of Medicines and HealthCare (EDQM). That sample was recrystallized from pure solvents or solvent mixtures of various polarity (acetone, acetonitrile, chloroform, dichloromethane, ethanol, ethyl acetate, 2-propanol, methanol, tetrahydrofuran, and water). Slow evaporation from acetone, chloroform, or dichloromethane at ambient temperature afforded colorless prismatic crystals, whereas acetonitrile/dichloromethane and methanol/dichloromethane produced colorless blocky crystals (the other solutions did not furnish crystalline material). From dichloromethane, occasionally the two phases crystallized concomitantly. Crystals of phase A (OXTB-A) were obtained from dichloromethane and from acetonitrile/dichloromethane and methanol/dichloromethane mixtures. For that purpose, the sample was first dissolved in a minimum quantity of acetonitrile or methanol, to which a larger quantity of dichloromethane was subsequently added. Phase A was obtained in two different habits: the crystals from dichloromethane and from mixed solvents were block-like in habit, whereas those that separated from methanol/dichloromethane mixture were prismatic. Form B (OXTB-B) was obtained as prismatic crystals by slow evaporation from dichloromethane, acetone, or chloroform.

4.2. Thermal Analysis. Early in this investigation (~1990), the initial DSC measurements were carried out on a prototype Mettler DSC/hot-stage (polarizing) microscope with (analog) photographic capability in the laboratory of Prof. J. D. Dunitz, ETH Zurich. This actually allowed the determination of the DSC of single crystals along with the observations of the thermosalient effects and the correlation of the phase change with morphology.

In the latter investigation, the DSC data were recorded on an SII EXTAR 6220 intrument at the National Institute for Materials Science, Tsukuba, at a heating rate of 5 K/min, in several temperature ranges. The two first heating−cooling cycles of the prismatic crystals of OXTB-A were identical, so no further cycling was required. The blocky crystals of OXTB-A exhibited slightly different transition temperatures between the first and the subsequent runs, so in that case six heating/cooling cycles were recorded (the absence of phase transitions at lower temperature was confirmed by an additional cycle between 180.15 and 275.15 K). The conditions used to record the thermoanalytical cuves are summarized in Table S8 in the Supporting Information.

4.3. IR Spectroscopy. The FTIR spectra were recorded from KBr pellets with a JASCO FT/IR-460 spectrometer. As the preliminary experiments indicated sensitivity of the spectra to the sample preparation procedure, the spectra of the as-received (commercial) OXTB, OXTB-A (blocky and prismatic crystals), and OXTB-B (obtained either by recrystallization from acetone or by thermal treatment of OXTB-A at 353.15 K and annealing during 5 min) were examined under a variety of sample preparation conditions. In each case, several spectra were recorded to ensure reproducibility. The effect of grinding on the spectra was monitored by periodic sampling of a material which had been ground for a longer time, pelleted, and recorded, until the spectrum remained constant on further grinding. The effect of UV irradiation was also studied. Because the IR spectra exhibited significant differences depending on whether the UV treatment was performed in the presence or in the absence of KBr, several procedures were employed: (i) a pure sample was irradiated with UV light from a 250 W medium-pressure Hg lamp (SP-7, Ushio), mixed with KBr, and then pelleted; (ii) a sample mixed with KBr was irradiated with UV light and subsequently pelleted; and (iii) a sample was mixed with KBr and pelleted, and then the pellet was irradiated with UV light. The heating was removed by using a heat filter (260−100 nm, HAF-50S-50H). Different UV powers and different exposure times (3−6 min) were applied.

4.4. Powder X-ray Diffraction. The X-ray powder diffraction patterns were measured at Boehringer-Ingelheim by Dr. D. Greenwood, using graphite-monochromated Cu Kα radiation ($\lambda = 1.54056$ Å) and an internal standard of fluorophlogopite. Form A was measured at room temperature and form B at 338 K.

4.5. Single-Crystal X-ray Diffraction. In Beer Sheva, the data for OXTB-A (300 K) were measured on a Syntex P-1 diffractometer with monochromated Mo Kα radiation ($\lambda = 0.71069$ Å) and a scintillation detector. The crystal was then removed to a Philips PW1100 diffractometer (at the Technion-Israel Institute of Technology) equipped with an Enraf Nonius FR 559 crystal heater for the data collection (at the same X-ray wavelength) at 327 and 331 K.

In Osaka, single crystals of polymorphs A and B were mounted on the goniometer of a Bruker APEX2 diffractometer equipped with a rotating anode source (Mo Kα radiation), a confocal multilayer X-ray mirror as monochromator, and a CCD as area detector. The

integrated and scaled[78] data were empirically corrected for absorption effects with SADABS.[79] The structures were solved by direct methods (SHELXS97).[80] The coordinates and anisotropic thermal displacement parameters for all non-hydrogen atoms were refined on F^2 by weighted full-matrix least-squares. All non-hydrogen atoms were refined anisotropically. Coordinates of hydrogen atom H4 on O4 were included as riding, while the torsion was refined from the electron density map (nearly identical positions were obtained by full refinement of the hydrogen atom position). All other H atoms were placed in geometrically idealized positions and constrained to ride on their parent atoms. The structure was refined with SHELXL97[81] implemented in the WinGX package.[82] The ORTEP-style molecular graphics were done with the program DIAMOND.[83] The complete data are provided in CIF files as Supporting Information. Crystallographic data for the structures have been deposited at the Cambridge Crystallographic Data Centre, 12 Union Road, Cambridge CB2 1EZ, UK (fax +44-1223-336033; E-mail deposit@ccdc.cam.ac.uk) and can be obtained on request, free of charge, by quoting the publication citation and the deposition numbers CCDC 780171−780174. Structure factor tables are available from the authors.

4.6. NMR Spectroscopy. ^{1}H and ^{13}C NMR spectra obtained in Beer-Sheva were measured at 298 K from $CDCl_3$ solutions on a Bruker WP-200-SY instrument. The ^{1}H NMR spectra obtained in Osaka were recorded in methanol-d_4 with with JEOL GSX instrument operating at 400 MHz.

4.7. Acoustic Spectroscopic Measurements. Acoustic measurements were carried out on a computerized Dunegan/Endevco 3000 spectrometer at the Nuclear Research Center Negev.

(78) *APEX2*, ver. 2.1-4, and *SAINT*, ver. 7.34A; Bruker AXS Inc.: Madison, WI, 2007.
(79) Sheldrick, G. M. *SADABS*; University of Göttingen: Göttingen, Germany, 1996.
(80) (a) Sheldrick, G. M. *SHELXS97*; University of Göttingen: Göttingen, Germany, 1997. (b) Sheldrick, G. M. *Acta Crystallogr.* **2008**, *A64*, 112–122. (c) Altomare, A.; Cascarano, G.; Giacovazzo, C.; Guagliardi, A.; Burla, M. C.; Polidori, G.; Camalli, M. *J. Appl. Crystallogr.* **1994**, *27*, 435–436.
(81) Sheldrick, G. M. *SHELXL-97*; University of Göttingen: Göttingen, Germany, 1997.
(82) Farrugia, L. J. *J. Appl. Crystallogr.* **1999**, *32*, 837–838.
(83) Brandenburg, K. *DIAMOND*, Ver. 3.1; Crystal Impact GbR: Bonn, Germany, 2005.

Acknowledgment. We are grateful to Dr. Dan Greenwood of Boehringer-Ingelheim for initially bringing this system to our attention and for supplying the original sample of the compound to Beer Sheva group, to Prof. Jack Dunitz at the ETH in Zurich for making his prototype DSC/microscope hot stage available to us, to Prof. Menahem Kaftory and Dr. Mark Botoshansky of the Technion-Israel Institute of Technology for making the single-crystal diffractometer with heating capabilities available, to Dr. Taketoshi Fujita from NIMS for the help with the DSC measurements, to Prof. Yosef Katz (NRCN) for the acoustic wave measurements, and to Prof. Robert Glaser of Ben-Gurion University for the NMR measurements. Work on part of this project was financially supported by the "Frontier Research base for Global Young Researchers" program of the Japan Science and Technology (JST) Agency. The visit of J.B. to Osaka University was generously supported by a Global COE program, "The Global Education and Research Center for Bio-Environmental Chemistry", from the Ministry of Education, Culture, Sports, Science and Technology, Japan.

Supporting Information Available: Weissenberg photograph of OXTB (Figure S1), overlapped structures of OXTB-B obtained by UV irradiation and by heating (Figure S2), calculated ^{1}H NMR chemical shifts (Figure S3), IR spectra of OXTB-A (Figure S4), ^{1}H NMR spectra of OXTB before and after the UV irradiation (Figure S5), crystal data and refinement details (Table S1), selected structural parameters (Table S2), solid-state ^{1}H NMR data for OXTB (Table S3), tables containing intramolecular parameters of phases OXTB-A and OXTB-B obtained by different methods (Tables S4−S7), experimental conditions used in the DSC analysis (Table S8), movies showing the thermosalient effects of rapidly heated crystals of OXTB (Movie S1) and of slowly heated single crystal of OXTB (Movie S2), and crystallographic data in CIF format. This material is available free of charge via the Internet at http://pubs.acs.org.

JA105508B